# Propagation of short electron pulses in underdense plasmas

N. Barov and J. B. Rosenzweig

*Department of Physics, University of California at Los Angeles, 405 Hilgard Avenue, Los Angeles, California 90024*

(Received 27 September 1993)

Dense relativistic electron beams traversing a plasma, in what is known as the underdense, or ion focusing, regime experience a strong, linear transverse restoring force. This force arises from the nearly immobile ions which form a channel of uncompensated positive charge when the plasma electrons are ejected in response to the introduction of the beam charge. This phenomenon can be used for focusing the electron beam to very high densities over long propagation distances. Several schemes have been proposed, including the nonlinear plasma wake-field accelerator, the adiabatic plasma lens, and the ion-channel laser, whose viability is based on this focusing effect for very short pulse, high current electron beams propagating in plasma. In this paper we examine, analytically and numerically, the self-consistent requirements on plasma density, beam current, length, and transverse emittance which must be satisfied in order for ion-channel formation and near equilibrium beam propagation to exist over the majority of the length of the electron beam. The dynamics of the beam-plasma system are modeled by a simultaneous solution of the plasma electron cold-fluid equations, and the Maxwell-Vlasov equation governing the beam's thermal equilibrium. The effects of introducing a strong axial magnetic field on the plasma response and beam equilibria are examined. In addition to developing criteria for self-consistent equilibrium focusing, a time-dependent analysis where the beam particles are treated as mobile particles in cells is developed in order to study the dynamical approach of this equilibrium. Inherently time-dependent phenomena, such as matching of the beam into the plasma and adiabatic lenses, are then examined with this method.

PACS number(s): 52.75.Di, 52.35.Mw, 52.40.Mj

## I. INTRODUCTION

When a high brightness relativistic electron beam is injected into an underdense plasma (having density less than that of the beam $n_b > n_0$), which for narrow plasma columns is termed the *ion focusing regime* (IFR), the plasma electrons can be ejected from the beam's path to form an ion channel. The leading edge (head) of the beam does not experience the full effects of the ion focusing, because the plasma electrons must take some finite time interval to move. On the other hand, once the plasma electrons are completely rarefied from the beam volume, the resulting uniform ion channel gives rise to a linear restoring force on the beam electrons. The focusing strength experienced by the electron beam due to this force is given for a round (cylindrically symmetric) beam by

$$K \equiv -\frac{F_r}{\gamma r m_e v_b^2} \simeq \frac{2\pi r_e n_0}{\gamma} , \qquad (1)$$

where $m_e$ and $r_e$ are the mass and the classical radius of the electron, respectively, $v_b$ is the axial velocity of the beam (assumed to be approximately equal to the total beam velocity), and the beam Lorentz factor $\gamma = [1 - (v_b/c)^2]^{-1/2}$. In this paper we are concerned with cases in the ultrarelativistic limit $v_b \simeq c$ ($\gamma \gg 1$). This type of focusing is one of the strongest attainable for high-energy electron beams, second perhaps only to the beam-beam forces found in a linear collider.

Electron beam propagation in the IFR has been studied extensively in the past decade [1–8], mainly in the context of relatively low-energy ($E_b = \gamma m_e c^2 \ll 100$

MeV), high current ($I_b > 1$ kA), and long pulse ($\sigma_t > 1$ ns) beams. In a long pulse beam, the transverse profile of the beam consists of three distinct regions [4]: a freely expanding beam *head*, a *pinch region* where the beam radius becomes smaller as the self-focusing of the beam in the plasma begins to assert itself, and a main *body* of the beam which has a constant radius, matched to the focusing strength of the ion channel. The transition between the pinch region, in which the plasma electrons are in the process of being expelled, and the ion channel is often termed the *pinch point*. The overall shape of the beam is trumpetlike, with the pinch point moving backwards in the beam frame as the beam head erodes.

For most of the cases previously considered, energy loss by the beam head (induction or plasma wake-field loss due to longitudinal electric force $-eE_z$) is often the limiting factor in determining the beam head erosion rate. In this paper we will be considering schemes typified by the ion-channel laser (ICL) [9] and the non-linear plasma wake-field accelerator (NPWFA) [10], in which the lengths characteristic of the beam's transverse stability (betatron wavelength, electron-hose growth length, etc.) are much smaller than the length over which appreciable energy loss,

$$L_E \simeq \frac{\gamma m_e c^2}{|-eE_z|_{\text{max}}} , \qquad (2)$$

occurs. In discussing the NPFWA (which, unlike the linear regime of the PWFA, involves very nonlinear plasma motion, in which the plasma electrons are completely ejected from the beam channel), for which the energy loss

rate for future experiments will likely be anywhere from 100 MeV/m to 1.5 GeV/m, we imply that we must only consider high-energy beams, $E_b > 20$ MeV. This said, from this point on we approximate the energy as a *constant* in our analysis, and consider only the effects of the beam's finite emittance when discussing erosion.

In the ICL, one needs very large currents in order to maximize the gain of the radiation produced, and in the NPWFA, high currents and short pulse lengths (less than a plasma period, typically a few picoseconds) are needed to drive large amplitude wake fields. In both of these schemes, the efficacy of the interaction is strongly dependent on how quickly past the head the beam passes through the pinch region—it should reach the pinch point before the maximum in current, to ensure that the beam head erosion does not cause a large portion of the beam charge to be deconfined past the ion-channel defined equilibrium radius.

In this paper, we examine the details of the pinch region evolution, with emphasis on determining the necessary conditions for achieving full ion-channel formation before the midpoint of a short electron pulse in the NPWFA. An approximate analytical model is developed in order to give some insight into the relevant physical parameters. In addition, previous particle-in-cell simulation work by Krall, Nguyen, and Joyce [4] has shown that for emittance-driven erosion, the pinch point moves very slowly and a near-equilibrium condition develops. Using this result as a guide, we develop a more sophisticated model in which the plasma electrons are described by fully relativistic cold-fluid equations and the beam physics is described by a Maxwell-Vlasov equilibrium. Both beam and plasma quantities are assumed to depend only on the distance from the head of the beam, and the equations are integrated from the beam head backwards. An axial magnetic field is also added to this system in order to provide a confining linear force, which prevents erosion of the beam head, and to give a reasonable, causal starting point in beam density for the integration of our equations. The effects of this field on both the beam and the plasma dynamics are examined.

Calculations concerning an equilibrium naturally must be justified by examining the physical mechanisms for formation of this equilibrium. By describing the beam as a set of super particles which are used to specify the beam current distribution, we can perform a time-dependent analysis of the beam-plasma interaction. The evolution of the beam distribution in time, or equivalently, as a function of propagation distance in the plasma, including emittance growth and formation of the trumpet-shaped beam head, are then examined.

Since the beam's pinch region and body must form equilibria which have very different characteristic beam radii, the evolution of the pinch region is, in general, a complex process which is dependent on the initial conditions. This brings into consideration the subject of matching the beam at the plasma boundary, a transition region of plasma density with a finite rise length. In turn, a relevant extension of this study is the subject of adiabatic focusing, in which the beam is compressed as the plasma density is raised slowly in the longitudinal direction.

## II. ANALYTICAL MODEL OF RAREFACTION

As stated above, in order for ion-channel focusing to be effective over the majority of the beam, the plasma electrons must be ejected by the leading edge of the beam. In this section, we examine the dynamics of the plasma electron motion in the presence of a beam, which is denser than the plasma, and derive a necessary condition for rarefaction to occur early in the beam passage time. To derive this condition, the beam transverse distribution is assumed to be that which would be obtained from matching into the focusing channel formed by the ions. Of course, this is only the case for the body of the beam; the details of the evolution of the beam head are examined below through numerical analysis.

Much of the analysis in this paper makes use of an envelope equation description of beam size evolution [5], or an equivalent approach based on Courant-Snyder parameters [6]. The envelope equation for a cylindrically symmetric beam in a uniform linear focusing channel is

$$\sigma_r'' + K\sigma_r = \frac{\epsilon^2}{\sigma_r^3} , \tag{3}$$

where $\sigma_r = (\overline{r^2})^{1/2}$. We will need to define the amplitude ($\beta$) function $\beta \equiv \overline{r^2}/\epsilon$, with the rms emittance (a constant under linear transport) $\epsilon = \sqrt{\overline{r^2 r'^2} - (\overline{rr'})^2}$. Upon substitution into the envelope equation, we have the equation

$$\beta'' + 2K\beta = \frac{1}{\beta}\left[\frac{\beta'^2}{2} + 2\right] . \tag{4}$$

The equilibrium size of an electron beam focused by a cylindrically symmetric ion column of charge density $en_0$ is found by noting that the equilibrium Courant-Snyder $\beta$ function is $\beta_{eq} = K^{-1/2}$, with $K$ as given by Eq. (1). In this case, one can identify the $\beta$ function as the inverse of the betatron wave number $\beta_{eq} = k_\beta^{-1} \equiv \lambda_\beta/2\pi$. The equilibrium rms radial beam size is thus

$$\sigma_{eq} = \sqrt{\beta_{eq}}\epsilon = \left[\frac{\epsilon_n}{\sqrt{2\pi r_e n_0 \gamma}}\right]^{1/2} , \tag{5}$$

where $\epsilon_n$ is the normalized rms emittance. Assuming the beam has a Gaussian profile in both longitude and radius, the peak beam density in equilibrium is thus

$$n_b = \frac{N_b}{(2\pi)^{3/2}\sigma_z\sigma_r^2} = \frac{N_b\sqrt{r_e n_0 \gamma}}{2\pi\epsilon_n\sigma_z} . \tag{6}$$

This beam density must be somewhat higher than $n_0$ (on which it is explicitly dependent) for the complete plasma rarefaction regime to be accessed. In order to determine when this rarefaction develops on a time scale, short compared to the beam pulse, a model of the plasma electron motion must be introduced.

In this regime of interest, where the plasma motion is mostly radial, the plasma electron dynamics can be well approximated by assuming that the total force on the plasma electrons is due only to the radial electric field of the bunch, which in the ultrarelativistic beam limit can be calculated by a simple application of Gauss's law. For

ease of analysis, we now approximate the beam density $n_b$ as uniform and, writing the plasma electron radial equation of motion with the distance from the head of the beam $\xi = ct - z$ as the independent variable, we have

$$r'' - k^2 r = 0 , \tag{7}$$

where

$$k^2 = 2\pi r_e n_b = \frac{k_p^2}{2} \left[ \frac{n_b}{n_0} \right] , \tag{8}$$

and the prime indicates a derivative with respect to $\xi$. Assumption of a temporal and longitudinal response dependent only on $\xi$ implies that we are ignoring transients which occur at the plasma boundary. Note that the form of the equations of motion are valid everywhere inside of the beam under our assumptions, which is the region we are concerned with. For a realistic beam profile (e.g., Gaussian), however, the expelling force rises less than linearly and Eq. (7) is valid only in the core of the beam.

The solution of Eq. (7) is, taking a plasma electron to be initially stationary at radius $r_0$,

$$r = r_0 \cosh(k\xi) . \tag{9}$$

Since the plasma electron density is proportional to the distance between electrons, expansion of these distances by a uniform factor (recall that we are ignoring longitudinal plasma motion) lowers the plasma density by the square of that factor, and

$$n(k\xi) = \frac{n_0}{[\cosh(k\xi)]^2} . \tag{10}$$

Requiring that the beam channel be rarefied, which we quantify by the condition $n(k\xi)/n_0 \leq 0.01$, we have, approximately, $k\xi > 3$. Although this result is derived assuming a constant current profile, we may use it to estimate the threshold for full rarefaction of the beam channel for a time-varying beam current by taking the integral of the wave number over time. In order to guarantee that the longitudinal center of a Gaussian beam is well focused, we have the (approximate) requirement

$$k\sigma_z > \frac{3}{\sqrt{2\pi}} . \tag{11}$$

For Gaussian beams, the fact that the expelling forces are smaller at the front of the pulse is offset by the gain in time allowed before the arrival of the beam center, mitigating the error introduced by our approximate arguments.

The condition for rarefaction of the beam channel given by Eq. (11) can now be used to estimate an expression for the self-consistent beam parameters needed for the major portion of the beam to be propagating in the ion-focusing regime. Squaring Eq. (11) and substituting into Eq. (8), we can write

$$\frac{n_b}{n_0} > \frac{9}{\pi(k_p\sigma_z)^2} . \tag{12}$$

Combining this result with the density expression in Eq.

TABLE I. Argonne Wake-field Accelerator beam parameters.

| Energy $E_b$ | 30–150 MeV |
|---|---|
| Electrons per bunch $N_b$ | $6 \times 10^{11}$ |
| Normalized emittance $\epsilon_n$ | 500 mm mrad |
| Bunch length $\sigma_z$ | 0.75–1.5 mm |
| Peak current $I_p$ | 10–20 kA |

(6), we have simply

$$N_b > \frac{9\epsilon_n}{\sqrt{\pi\gamma} r_e(k_p\sigma_z)} . \tag{13}$$

This expression has direct implications for short pulse beam propagation in plasma. For a symmetric Gaussian beam pulse, which is used to drive a nonlinear plasma wave field, we have the limit on beam length $k_p\sigma_z < 2$, which is required in order for the wake field not to be diminished by the oscillatory plasma response. Note that for asymmetric longitudinal profile beams, this corresponds to a limit only on beam fall length, not the rise length. In addition, as can be seen from Eq. (11), if we choose $k_p\sigma_z > 2$, then the result is not *necessarily* valid, as we would then be allowing the possibility that $n_b < n_0$. Thus, subject to this constraint, $k_p\sigma_z \leq 2$, we have

$$N_b > \frac{9\epsilon_n}{\sqrt{4\pi\gamma} r_e} . \tag{14}$$

This condition, which is now independent of plasma density and beam length, is not easy to satisfy. However, new, high current, high brightness electron sources based on rf photocathode technology should produce beams which satisfy Eq. (14). In particular, an accelerator facility currently undergoing commissioning, the Argonne Wake-field Accelerator (AWA, the parameters of which are shown in Table I), should yield a beam which satisfies this inequality by more than an order of magnitude. Initial tests of the NPFWA are to be performed at the AWA, with construction of the experiments presently underway.

The arguments supplied here clearly ignore the complications of the pinch region dynamics and are therefore a necessary, but not sufficient, condition for attaining ion-focused confinement of a short pulse electron beam. In order to examine the requirements for reaching this plasma electron "blow-out" regime, we must use a more sophisticated model. In Sec. III, we discuss a cold-fluid description of the plasma electron motion as a first step in a full analysis of the beam-plasma system.

## III. COLD-FLUID DESCRIPTION OF PLASMA MOTION

Since the plasma electron motion excited by a beam which is much denser than the plasma is inherently nonlinear, it is not amenable to simple analytical description. Computer simulations have shown, however, that for the initial half-cycle (the blow out of the electrons) of the plasma oscillation, the plasma electron motion is nearly

laminar. Thus the cold-fluid description is a good approximation to the plasma electron response for the situation of interest here. While the fluid equations cannot be solved analytically, they can be easily integrated numerically. This approach was originally developed by Breizman *et al.* for use in plasma wake-field analysis [11]. Here, we extend this numerical approach to include the field of the focusing solenoid and a Maxwell-Vlasov treatment of the near-equilibrium beam dynamics.

The relativistic equation of motion for an electron cold-fluid element,

$$\frac{\partial \mathbf{p}}{\partial t}+(\mathbf{v}\cdot\nabla)\mathbf{p}=-e\left[\mathbf{E}+\frac{1}{c}(\mathbf{v}\times\mathbf{B})\right] , \tag{15}$$

combined with the continuity equation,

$$\frac{\partial n}{\partial t}+\nabla\cdot(n\mathbf{v})=0 , \tag{16}$$

has been generalized, in our case, to account for rotation of the plasma electrons around the beam axis due to the effects of the axial magnetic field. We assume a rotationally symmetric solution so that $d/d\theta=0$, where $\theta$ is the azimuthal angle in the cylindrical coordinate system. Equations (15) and (16), as well as the Maxwell equations,

$$\nabla\times\mathbf{B}=\frac{4\pi}{c}\mathbf{J}+\frac{1}{c}\frac{\partial\mathbf{E}}{\partial t} , \tag{17}$$

$$\nabla\times\mathbf{E}=-\frac{1}{c}\frac{\partial\mathbf{B}}{\partial t} , \tag{18}$$

with $\mathbf{J}=-e(n\mathbf{v}+n_b\mathbf{v_b})$, are solved forwards in $\xi$, starting causally ahead of the beam in the region of unperturbed plasma. The boundary condition in the radial direction is that of a conducting wall at radius $r_c$ at the edge of the computational grid. It is also assumed that the beam is propagating at the speed of light. The errors in determination of the fields resulting from this assumption are of order $\gamma^{-2}$.

The beam particles are treated as paraxial rays for the purpose of integrating Eqs. (15)–(18). In particular, we specify that the beam velocity $\mathbf{v_b}=c\hat{\mathbf{z}}$ and assume that the beam gives no important contributions to the total radial or azimuthal current density.

## IV. BEAM DISTRIBUTION: MAXWELL-VLASOV EQUILIBRIUM MODEL

The description of an electron beam propagating in the ion-focused regime discussed in Sec. I, based in large part on the results of Ref. [4], assumes that the beam is initially matched to the channel (there are no envelope oscillations within the body of the beam), and that a near equilibrium develops in the pinch region, giving the characteristic trumpet shape of the beam's spatial profile. In our present model of the beam equilibrium we do not include energy variations in the beam, muting the issue of inductive erosion, and the emittance-driven erosion is stabilized by the applied axial magnetic field, making the situation an even better approximation to an equilibrium case.

In order to incorporate the effects of the transition between the head of the beam, confined only by the relatively weak focusing of the solenoid, and the body of the beam, which is well confined by the ion focusing in the rarefaction channel, we adopt a Maxwell-Vlasov description of the beam, which assumes that each infinitesimal longitudinal "slice" of the beam is in equilibrium with the focusing fields.

To argue for the applicability of the model it is useful at this point to discuss how this equilibrium may come about, with a more detailed treatment given below. For the beam body there is no inherent problem, as one can envision that it is initially matched to the linear focusing of the ion channel upon entry into the plasma. In the pinch region, however, the plasma focusing fields are nonlinear, and of course weaker than those in the ion channel itself. We can therefore expect that the beam distribution in the pinch region will evolve without binary collisions in a few betatron oscillations into a near equilibrium by phase mixing due to the amplitude dependence of the oscillation frequency. The collisionless damping of the beam profile oscillations comes at the price of the filamentation of the transverse phase space or, equivalently, emittance growth. In order to expedite the analysis, we assume that this growth, which is difficult to calculate since it involves solving the microscopic equations of motion, is negligibly small for most of the beam population. Also, the initial condition of matching the beam envelope to the ion focusing will cause the forward edge of the beam, which only experiences the solenoidal focusing, to undergo undamped betatron oscillations. This effect can be ignored, since there is a very small population of particles involved. The collisionless approach to equilibrium, and accompanying emittance growth in overdense ($n_b < n_0$) plasma focusing, is discussed in detail in Ref. [12].

This model is suitable for describing a near-equilibrium state of the beam, which we assume comes about after the initial transient effects have dissipated. The effects of the axial magnetic field are employed mainly to produce a "startup" density at the beam head, which we set equal to the equilibrium (no betatron oscillations) density in the axial magnetic field. The time-independent Maxwell-Vlasov equation is written

$$\frac{p_r}{\gamma m}\frac{\partial f(r,p_r)}{\partial r}=-F_r(r)\frac{\partial f(r,p_r)}{\partial p_r} , \tag{19}$$

where $p_r$ is the momentum and $F_r(r)=-e(E_r-H_\theta)$ is the radial force on a paraxial particle moving near the speed of light. In this calculation, the maximum in phase space density $f(0,0)$ is constant and the distribution function is assumed smooth and separable in $r$ and $p_r$, as we are ignoring phase space filamentation effects. Equation (19) is solved by radial integration [once each longitudinal ($\xi$) step] in order to provide the inhomogeneous driving term for the plasma dynamics in Eq. (18) at the following time step. It should be noted that for an ultrarelativistic beam the net self-force vanishes, and $F_r$ arises only from the plasma and externally applied magnetic fields. Computationally, Eq. (19) reduces to the usual uncorrelated Gaussian distribution when the focus-

ing force is linear (as in the IFR) and to the Bennett profile when the beam is much less dense than the plasma, and narrow compared to $k_p^{-1}$. Appendix B discusses the numerical techniques used in evaluating the transverse density profile.

## V. BEAM EQUILIBRIUM: COMPUTATIONAL RESULTS

The simultaneous numerical solution of the cold-fluid equations with the Maxwell-Vlasov equation for the self-consistent beam equilibrium allows us to examine the applicability of our analytical model. However, the addition of the axial magnetic field of strength $B_z$, which for an ultrarelativistic beam gives a focusing strength,

$$K_{\text{sol}} \simeq \left[ \frac{eB_z}{2\gamma m_e c^2} \right]^{1/2}, \tag{20}$$

to provide a starting equilibrium distribution at the beginning of the beam, presents a problem if the initial beam head radius,

$$\sigma_{\text{sol}} = \left[ \frac{2m_e c^2 \epsilon_n}{eB_z} \right]^{1/2}, \tag{21}$$

is much larger than a plasma skin depth $k_p^{-1}$. In this case, the plasma return current flows inside of the beam, negating the magnetic self-focusing forces of the beam. Under this type of initial condition, the self-focused equilibrium in the underdense regime is never achieved in our model. This situation is, of course, a spurious artifact of the model, and in order to avoid it we set the magnetic field in these calculations to give $k_p \sigma_{\text{sol}} \leq 2$. In practice, the beam will be injected into the plasma near the equilibrium beam size corresponding to the ion focusing, not the solenoid focusing, and so the value $\sigma_{\text{sol}}$ is of only marginal importance to the final state of the beam equilibrium.

Of course, the addition of a longitudinal magnetic field changes the plasma electron dynamics somewhat, in particular making it more difficult to eject them from the beam channel. This is a relatively small effect as long as the electron plasma frequency is much larger than the cyclotron frequency, $\omega_p \gg \omega_c$. This is in fact the case for all plasma densities and applied magnetic fields of interest. It should be noted in this regard that all past and planned plasma wake-field acceleration experiments employ solenoidal magnetic fields for confining the ambient plasma [13].

The scaling (in the variables $N_b$, $\epsilon_n$, and $k_p \sigma_z$) for achieving rarefaction of the plasma electrons set forth in Eq. (13) has been explored using this computational model. The results of varying the total charge in the bunch, while holding other variables constant [$\epsilon_n = 400$ mm mrad, $k_p \sigma_z \simeq 2$, $\sigma_z = 1$ mm ($n_0 = 10^{14}$ cm$^{-3}$), and $\gamma = 300$], is shown in Fig. 1, which plots a normalized measure of the beam spot area, i.e., the on-axis equilibrium density which would be due to the ion-channel focusing, divided by the calculated density, as a function of $k_p \xi$. It can be seen that the plasma is nearly totally rarefied at the beam's longitudinal center for all bunch populations over $1.2 \times 10^{11}$. This is slightly more pes-
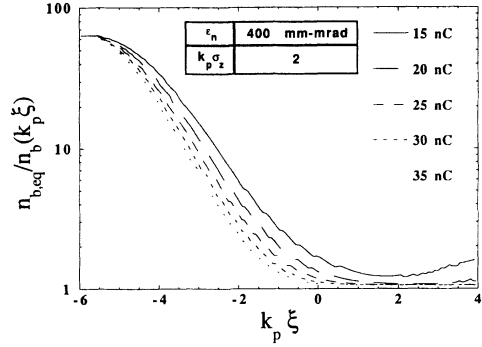


FIG. 1. Normalized beam spot area (defined as a function of longitudinal position by $n_{\text{eq}}/n_b(k_p \xi, 0)$, with $n_{\text{eq}} = N_b \exp(-\xi^2/2\sigma_z^2)/[(2\pi)^{3/2}\sigma_{\text{eq}}^2 \sigma_z]$, for a number of different bunch charges with other parameters held constant ($\epsilon_n = 400$ mm mrad, $k_p \sigma_z = 2$, $\gamma = 300$, and $\sigma_z = 1$ mm).

simistic than the result obtained from Eq. (13), which predicts that $2.4 \times 10^{10}$ should be sufficient. This is to be expected, since we have relaxed the assumption that the beam head and pinch regions are focused to $\sigma_{\text{eq}}$.

In Fig. 2, we display the results of varying the emittance while holding the other beam parameters ($N_b = 6 \times 10^{10}$, $k_p \sigma_z = 2$, $\gamma = 300$, and $\sigma_z = 1$ mm) constant. According to Eq. (13), rarefaction at the middle of the beam should be achieved for all emittances smaller than 120 mm mrad, while in Fig. 2 we can see that at 100 mm mrad the rarefaction has already deviated from completion. This disagreement is again due to the analytical model being too optimistic in its assumptions concerning the beam head density.

Figure 3 shows the parametric dependence of the rarefaction condition on plasma density in order to reveal the effects of varying the quantity $k_p$. The normalized beam spot size is plotted as a function of $\xi$ for a beam with parameters $N_b = 6 \times 10^{10}$, $\gamma = 300$, and $\sigma_z = 1$ mm. Only the case with $n_0 = 10^{14}$ cm$^{-3}$ ($k_p \sigma_z = 1$) rarefies well, as has been anticipated. For smaller plasma densities, the focusing is not strong enough to focus the beam to much higher density than the plasma density, and in turn, the
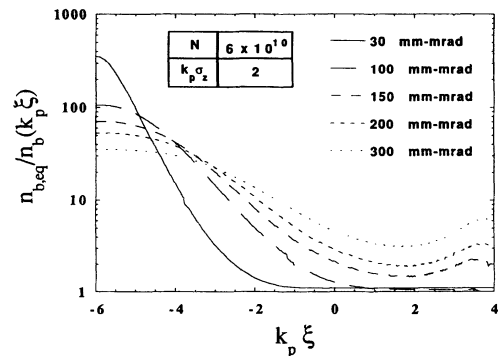


FIG. 2. Normalized beam spot area, as defined in Fig. 1, for a number of different emittances with other parameters held constant ($N_b = 6 \times 10^{10}$, $k_p \sigma_z = 2$, $\gamma = 300$, and $\sigma_z = 1$ mm).
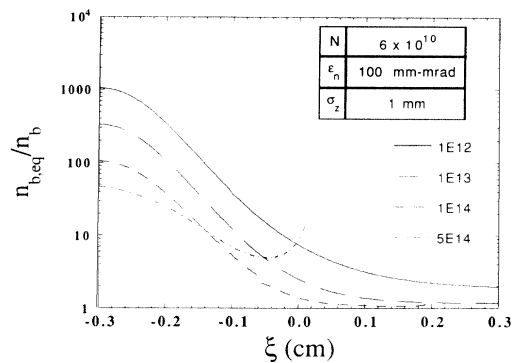
FIG. 3. Normalized beam spot area as a function $\xi$, as defined in Fig. 1, for a number of different plasma densities with other parameters held constant ($N_b = 6 \times 10^{10}$, $\gamma = 300$, $\epsilon_n = 100$ mm mrad, and $\sigma_z = 1$ mm).

plasma electrons are not expelled as quickly by the beam density. For much larger densities, the plasma has time to respond to the beam charge and the beam is well focused, but simply not denser than the plasma.

## VI. DYNAMICAL APPROACH TO BEAM EQUILIBRIUM

The validity of the equilibrium beam model developed in the previous sections is dependent on the initial mismatch of the pinch region dissipating through collisionless damping. In order to provide a more solid underpinning for the Maxwell-Vlasov model, we now examine the approach to this equilibrium by allowing the beam current distribution to have an explicit time dependence. This is accomplished by representing the beam current as a system of "super particles" and assigning currents to the computational grid associated with the plasma electron fluid equations based on the position of these super particles. At each time step the fluid equations are solved based on these beam currents, and the beam particle positions and momenta are updated based on the focusing fields due to the plasma response. This scheme is thus a rudimentary type of a particle-in-cell calculation. It is also reminiscent of previous approaches to IFR propagation analysis, the multicomponent model developed by Sharp, Lampe, and Uhm [14], and the spread-mass model credited to Lee [15]. Unlike these models, however, we are not attempting to introduce a tool which directly aids theoretical analysis, but are merely using the super particles to calculate the microscopic dynamics of the beam particles in a straightforward manner.

In order to mitigate statistical fluctuation effects in the representation of the beam current, there must be a sufficient number of super particles in each $\xi$ slice, which in these calculations is taken to be 50. The beam particles are initialized as the bi-Gaussian distribution in each transverse phase space plane that is matched to the linear focusing which would be obtained from a uniform ion column to given an rms beam size of $\sigma_{eq}$ [5].

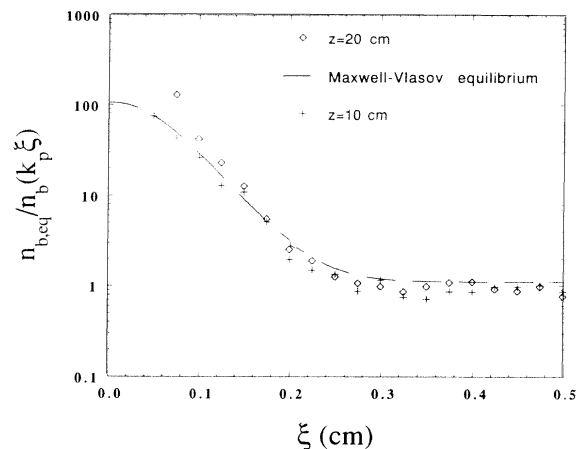These calculations are valid only in the limit where the



FIG. 4. Comparison of Maxwell-Vlasov equilibrium prediction with time-dependent beam model (at $z = 10$ and 20 cm into the plasma), with the on-axis beam density as a function of $\xi$ normalized to that obtained from ion-channel equilibrium. The beam-plasma system has the following parameters: $N_b = 1.2 \times 10^{11}$; $E_b = 25$ MeV; $\epsilon_n = 100$ mm mrad; $k_p \sigma_z = 2$; $k_p \sigma_{sol} = 2$; and $\sigma_z = 1$ mm.

beam parameters at a given $\xi$ slice change in time much more slowly than the plasma parameters. This is equivalent to requiring that $k_\beta = k/\gamma \ll k_p$, or that $\gamma \gg 2$, which we have already assumed to be the case.

The comparison of the Maxwell-Vlasov equilibrium prediction with that obtained from the time-dependent super particle model of the beam is shown in Fig. 4. The effective normalized beam spot size, as a function of $\xi$, is shown for the equilibrium calculation and for the time-dependent calculation at $z = 10$ and 20 cm into the plasma. In this case, the beam-plasma system has the following parameters: $N_b = 1.2 \times 10^{11}$, $E_b = 25$ MeV, $\epsilon_n = 100$ mm mrad, $k_p \sigma_z = 2$, $k_p \sigma_{sol} = 2$, and $\sigma_z = 0.75$ mm. In order to isolate the transverse effects, the energy loss of the beam particles due to the inductive $E_z$ is again ignored. One can see that the agreement is quite good in the body of the beam and in the pinch region. The extreme beam head shows some oscillation, however, due to the mismatch induced by initially focusing the entire beam down to the equilibrium ($\beta_{eq} \simeq 5$ mm) attained by the beam body. The distribution of the head particles, which perform large oscillations around the equilibrium provided by the solenoid, does not seem to greatly affect the distribution in the pinch and body regions.

## VII. BEAM MATCHING

The launching of a beam into the plasma with a predefined state of ballistic propagation, as was done in Sec. VI, ignores the issues surrounding the negotiation of the plasma boundary region, where $n_0(z)$ rises from zero to its final value in the bulk of the plasma. This transient effect must be examined carefully in order to match the beam's transverse propagation characteristics to the ion channel. In addition, by allowing the plasma boundary to aid in matching, one should be able to mitigate the os-

cillations of the beam head, as it need not be initially as tightly focused.

We will perform an analysis which contains the plasma response below by employing an extension of the numerical modelling techniques developed in Sec. VI. First, however, it is instructive to explore an analytical model of the beam propagation assuming (as is frequently done in IFR propagation analyses) that the focusing experienced by the beam is given simply by the ion density, that is,

$$K(z) \simeq \frac{2\pi r_e n_0(z)}{\gamma} . \tag{22}$$

In order to define this model completely, we must now specify the plasma density profile. We require that the density be zero outside of a certain finite region, and additionally, to avoid any spurious transients in the solution to Eq. (22), we also require that the first derivative of the density be continuous. We choose a simple, mathematically tractable and physically reasonable ramped plasma density profile,

$$n_0(z) = 0, \quad (z < 0) ,$$

$$= n_m \sin^2(k_r z) \quad \left[ 0 \le z < \frac{\pi}{2k_r} \right] , \tag{23}$$

$$= n_m \quad \left[ z \ge \frac{\pi}{2k_r} \right] . \tag{24}$$

In the plasma boundary region (the *ramp*, $0 \le z < \pi/2k_r$), the equation of motion for the beam particles in either transverse dimension is of the same form,

$$\frac{d^2 x}{dz^2} + K_0 \sin^2(k_r z) x = 0 , \tag{25}$$

where the constant $K_0 = 2\pi r_e n_m / \gamma$. Note that Eq. (25) is formally the Mathieu equation (15) in the region of the rising density.

Use of the Mathieu form guides the discussion of the matching problem. For example, we may look for solutions that match a waist (that is $d\sigma_x/dz = 0$) at $z = 0$ to a waist at the end of the boundary region $z = \pi/2k_r$. For this to be true, any ray which is initially parallel must either be parallel or cross the $x = 0$ plane at $z = \pi/2k_r$. In addition, any initially on-axis ray must be either parallel or return to the $x = 0$ plane at $z = \pi/2k_r$. In short, we require simultaneous odd and even periodic solutions to the Mathieu equation. However, the theory of Mathieu equations explicitly denies this possibility, since the odd and even solutions have distinct frequencies (that is, $K_0$ must be different for the two types of solutions) [16]. Thus the beam strictly must not be at a waist at the beginning of a ramp, but in fact must be converging to achieve a match at $z = \pi/2k_r$.

In practice, the best way to derive the initial conditions at the beginning of the ramp is to start with the desired match at $z = \pi/2k_r$ and solve the envelope equation for the rms beam size,

$$\frac{d^2\sigma}{dz^2} + K_0 \sin^2(k_r z)\sigma = \frac{\epsilon^2}{\sigma^3} , \tag{26}$$

backwards in $z$. In keeping with the previous discussion, we can classify the ramped profiles according to the phase advance,

$$\psi \equiv \int_0^{\pi/2k_r} \frac{dz}{\beta(z)} = \int_0^{\pi/2k_r} \frac{\epsilon}{\sigma^2(z)} dz , \tag{27}$$

which is approximately $n\pi/2$, with $n$ equal to a positive integer. For example, the shortest ramp has an approximate phase advance of $\pi/2$, corresponding to a quarter of a betatron oscillation; an initially parallel ray approximately comes to a focus at $z = \pi/2k_r$.

We can exploit our time-dependent model of the plasma fluid response under certain conditions. The first is that the plasma conditions do not change appreciably over the distance from the head to the tail of the beam, which can be quantified by requiring $k_r \sigma_z \ll 1$. This is satisfied in all the calculations given below, since the beam length is typically 1 mm, while the rise length is several centimeters. In addition, there is a less relevant requirement mainly concerning calculation of the wake fields behind the beam, $k_p \gg k_r$, which is satisfied for the denser regions of the plasma (which are cases of interest, since $k_p \simeq \sigma_z^{-1}$).

The matching of the beam body, which is here defined to be the last half of the beam, is illustrated in Fig. 5. In this case, the ramp is 1.63 cm long ($k_r = 0.964$ cm$^{-1}$), corresponding to $\psi \simeq \pi/2$. The beam-plasma system has the same parameters as in Fig. 4. The mismatch and error in $\sigma_{eq}$, which for this system should be 102 microns, is due only to numerical inaccuracy of the plasma-derived focusing force. It should be noted that the beam has a virtual waist (that which is obtained if the plasma is removed) of 123 $\mu$m, which is not much larger than the ion-channel equilibrium. Thus the matching section in this case does little to suppress beam head oscillation and loss.

As an example of a matching section which allows the initial external focusing to be eased (since the virtual waist is larger), we examine a longer ramp in which $\psi \simeq \pi$. The virtual waist in this case is 149 $\mu$m, and so the
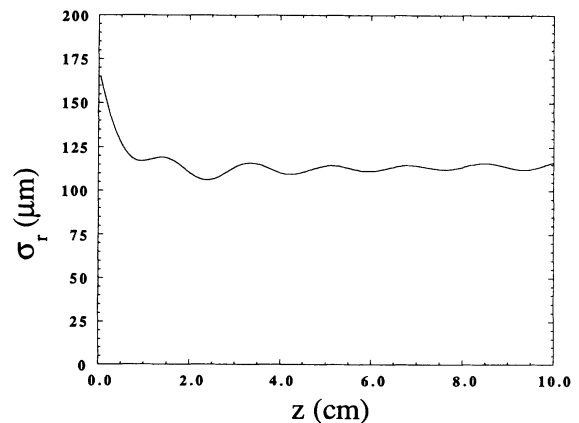


FIG. 5. Matching of the beam body (the last half of the beam) with the ramp of length 1.63 cm ($k_r = 0.964$ cm$^{-1}$), corresponding to $\psi \simeq \pi/2$. The beam-plasma system has the same parameters as in Fig. 4.
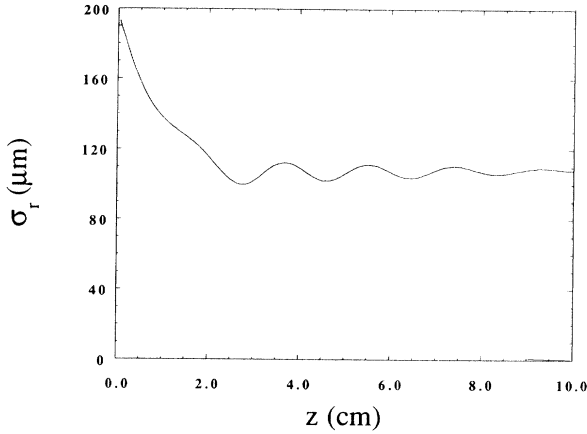
FIG. 6. Matching of the beam body with the ramp of length 3.33 cm ($k_r = 0.472$ cm$^{-1}$), corresponding to $\psi \simeq \pi$. The beam-plasma system has the same parameters as in Fig. 4.



FIG. 7. Adiabatic focusing of the beam body, with an exponential rise in plasma density from $n_0 = 10^{12}$ cm$^{-3}$ to $n_0 = 10^{14}$ cm$^{-3}$ in a length 7 cm ($\kappa = 0.657$ cm$^{-1}$). In this case, the beam parameters are $N_b = 6 \times 10^{11}$, $E_b = 150$ MeV, $\sigma_z = 1$ mm, and $\epsilon_n = 400$ mm mrad, with initial conditions $\sigma_0 = 483$ $\mu$m and $\alpha_0 = 0.7$.

depth of the initial focus is over twice $\beta_{eq}$. The evolution of the rms transverse size of the beam body is shown in Fig. 6. The collisionless damping of the beam size oscillations indicates the presence of some deviation from constant, linear focusing in the bulk of the plasma.

## VIII. ADIABATIC FOCUSING

If the subject of long matching sections is explored to its logical conclusion, it becomes quite similar to what has been termed "adiabatic focusing," in which the plasma density, and thus the focusing strength, is ramped over many orders of magnitude. In addition, the beam is initially nearly matched to the focusing strength and remains so throughout the ramp, producing a beam which is also many orders of magnitude denser at the end of the ramp. It has been proposed by Chen et al. [17] that this method of focusing could alleviate the effects of radiation-induced aberrations in linear collider final focusing systems (the Oide effect [18]).

In Chen's paper on adiabatic focusing, the measure of adiabaticity, $\alpha \equiv -(\frac{1}{2}) d\beta/dz$, is taken to be less than unity. In fact the optimum ramp in focusing strength may be optimally much larger than 1. If this is the case, the focusing strength must rise in $z$ with a uniformly positive second derivative, to insure that the beam envelope does not undergo wild oscillations. In fact, Chen et al. choose a plasma density that is singular at the end of the ramp. A discussion of the optimization (from the point of view of the beam dynamics) of the ramp by Williams and Katsouleas [19] yields a more physical density profile. For our purpose, that of investigating the self-consistency of the beam-plasma system [20], we choose a simpler, more experimentally realizable density which satisfies our requirements on the functional form of the focusing strength increase,

$$n_0(z) = n_0(0) \exp(\kappa z) , \qquad (28)$$

with the beginning of the plasma region at $z = 0$. For our calculational model to be valid in this system, we must
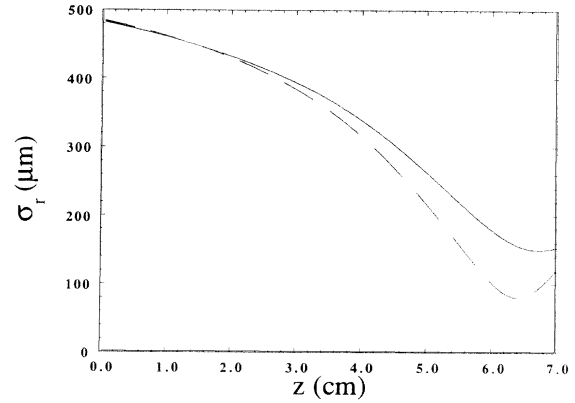
have $\kappa \sigma_z \ll 1$ and $\kappa \ll k_p$. The last (less relevant) condition is again problematic at lowest densities. More important than the validity question is the issue of self-consistent blowout of the plasma electrons in the low density region. The inequality given in Eq. (13), which predicts the self-consistency condition for $\alpha < 1$, can only be satisfied over a limited range of plasma densities. For the Argonne experiment, the inequality is satisfied maximally by a factor of 30 for $k_p \sigma_z = 2$, which means that a ramp of three orders of magnitude leading to the condition $k_p \sigma_z = 2$ will still be self-consistent.

A case where the beam self-consistently is compressed by a long ramped underdense lens is shown in Fig. 7, which displays the rms size of the beam body (as defined for Figs. 5 and 6) for two sets of initial conditions. The exponential ramp, which is 7-cm long, begins at $n_0 = 10^{12}$ cm$^{-3}$ and ends at $n_0 = 10^{14}$ cm$^{-3}$. The case shown in the solid line is a beam with an initial correlation of $\alpha_0 = 0.7$ (the virtual waist is $\sigma = 410$ $\mu$m). The beam comes to an approximate waist of $\sigma = 150$ $\mu$m at the end of the plasma, as is quantitatively predicted by the solution of Eq. (26). This agreement indicates that rarefaction has been indeed achieved for the body of the beam. This case is a nearly adiabatic lens, as $\alpha$ peaks at a value of 1.6. As one would expect for a ramp of two orders of magnitude in plasma density, the beam becomes about a factor of 10 denser at the end of the lens.

While the plasma dynamics work well in this case, the nearly adiabatic condition implies that the beam dynamics will be a sensitive function of initial conditions. To illustrate this phenomenon, $\alpha_0$ is increased by 10% in the case illustrated by the dashed line. Although the focusing is still effective (the blowout regime is accessed well), the beam body envelope and its first derivate deviate quite a bit from the previous case.

## IX. CONCLUSIONS

The analytical, Maxwell-Vlasov, and simulational models introduced in this work have been shown to give a

consistent view of the requirements on a short beam-plasma system for propagation in the ion-focused or blow-out regime. As can be seen from the included examples and from the extension of the simulational model to include beam matching and adiabatic focusing, obtained results have proven to be of significant help in addressing issues surrounding the experimental testing of the NPWFA and related phenomena.

The methods employed in this paper could be used to deduce further interesting results. For instance, one can enhance the efficiency of the NPWFA by ramping the beam's longitudinal profile [10] slowly, $k_p \sigma_{rise} \gg 1$, if the fall length is still maintained to be shorter than a few $k_p \sigma_{fall} < 2$. The scaling laws developed in this paper will be extended to cover this asymmetric beam case in future work. Additionally, for either long rise length beams or very dense beams, $n_b \gg n_0$, the issue of ion motion becomes relevant. This can be straightforwardly examined by treating the ions as a cold fluid; the results of this study will be presented in a forthcoming work.

Other important issues, such as dipole instabilities of the beam-plasma system [20], lie completely outside of the scope of this paper, as they cannot be addressed within the axisymmetric models employed here. A likely candidate for posing trouble is the electron-hose instability, which in the long electron pulse limit has a very fast growth rate. For a very short pulse length however, the return sheath dynamics must be treated relativistically, and the analysis is not so simple. This issue, along with the general question of instabilities in the NPWFA, will also be studied in future work.

### ACKNOWLEDGMENTS

### APPENDIX A: NUMERICAL SOLUTION OF PLASMA BEHAVIOR

The numerical solutions of the fluid equations which we have employed rest on the work of Breizman et al. [11] who have used the approach of applying the speed of light phase velocity condition $\partial/\partial z = -\partial/\partial ct$ to Eqs. (15)–(18). We have extended this approach to allow the rotation of the plasma electrons induced by the applied solenoidal field $H_{z0}$, which necessitates solving for $H_r$,

TABLE II. Numerical code variables in terms of physical quantities.

| Simulation variable | Relation |
| --- | --- |
| $V_i$ | $= v_i'/(c - v_z')$ |
| $E, H$ | $= E' m_e \omega_p c/e (, = H' m_e \omega_p c/e)$ |
| $p$ | $= m_e cp'$ |
| $t$ | $= \omega_p t'$ |
| $n$ | $= n'/n_0$ |

$E_\phi$, and $H_z$, as well as the inclusion of a centrifugal force term. The variables used in the simulation are dimensionless. Table II shows how these are related to the physical (primed) quantities.

Using these variables, the fluid equation becomes

$$\frac{\partial}{\partial t}V_r + V_r\frac{\partial}{\partial r}V_r$$
$$= G[V_r E_z + H_\phi + (1 + V_z - V_r^2)(E_r - H_\phi + F_c)$$
$$+ V_\phi H_z],$$

$$\frac{\partial}{\partial t}V_z + V_r\frac{\partial}{\partial r}V_z = G[(1+2V_z)E_z + V_r H_\phi \qquad (A1)$$
$$- V_r V_z(E_r + F_c - H_\phi) - V_\phi H_r],$$

$$\frac{\partial}{\partial t}V_\phi + V_r\frac{\partial}{\partial r}V_\phi = G[V_\phi E_z + V_r V_t(H_\phi - E_r - F_c)$$
$$- V_r H_z - H_r],$$

$$G = \sqrt{1 + 2V_z - V_r^2}, \qquad (A2)$$

with the centrifugal force equal to

$$F_c = \frac{V_\phi^2}{r(a - V_z)\sqrt{1 - V_r + 2V_z}}. \qquad (A3)$$

The continuity equation becomes

$$\frac{\partial}{\partial t}N + \frac{1}{r}\frac{\partial}{\partial r}(rNV_r) = 0. \qquad (A4)$$

Again using the speed of light phase velocity condition $\partial/\partial z = -\partial/\partial t$, the Maxwell equations become

$$\frac{\partial}{\partial r}\frac{1}{r}\frac{\partial}{\partial r}(rH_\phi) = \frac{\partial}{\partial t}(NV_r) + \frac{\partial}{\partial r}(NV_z) + \frac{\partial}{\partial r}J_b, \qquad (A5)$$

$$\frac{\partial}{\partial t}(E_r - H_\phi) = -NV_r, \qquad (A6)$$

$$\frac{\partial}{\partial r}\frac{1}{r}\frac{\partial}{\partial r}rH_r = -\frac{\partial}{\partial t}NV_\phi, \qquad (A7)$$

$$\frac{\partial H_z}{\partial r} = -NV_\phi. \qquad (A8)$$

It is unnecessary to have a separate equation for $E_\phi$ because it is trivially related to $H_r$ ($E_\phi = -H_r$). The plasma is assumed to be surrounded by a conducting cylinder at the edge of the computational grid. At this radius, the quantities $H_r$, and $E_z$ must tend to zero. Therefore, the equations for these fields are integrated starting from the maximum radius. Also, the flux associated with $H_z$ through this tube must be conserved. The evolution of $H_z$ is computed in the usual way, but an offset is added to this field which preserves the flux. Well ahead of the beam, $H_z$ is set equal to the field of the solenoid, thereby defining the initial flux. All other fields are assumed to be zero by symmetry. The discrete form of these equations is applied to give the fields after one step in $\xi$. All of the equations are discretized in a straightforward manner except Eqs. (32) and (33). The discrete form of the continuity equation, for example, takes the form,

$$N_i(z+dz) = \frac{1}{2r_i} \left[ r_{i+1}N_{i+1} + r_{i-1}N_{i-1} \right.$$

$$\left. - \frac{dz}{dr}(r_{i+1}J_{ri+1} - r_{i-1}J_{ri-1}) \right] ,$$

$$J_r = NV_r . \quad \text{(A9)}$$

## APPENDIX B: MAXWELL-VLASOV BEAM-PLASMA EQUILIBRIUM

It is the purpose of this appendix to outline the numerical methods used to compute the transverse equilibrium of the beam. The usual solution of the time-independent Vlasov equation involves making some assumption about the behavior of the focusing force as a function of radius. In our numerical work, this force is that experienced by a paraxial relativistic electron due to the plasma fields in the combination $F_r = -e(E_r - H_\theta)$, and the additional external focusing force provided by the solenoid. As the rotation induced by the solenoidal focusing is second order in field strength, we ignore its diamagnetic contribution to the longitudinal magnetic field. Likewise, we also ignore space charge forces of the beam, which are small, on the order of $\gamma^{-2}$.

Using the equilibrium Vlasov prescription, the phase space distribution is taken to be

$$f(r,p_r) = \frac{N_b}{(2\pi)^{3/2}\sigma_z p_z \epsilon} \exp[-aV(r)] \exp\left[\frac{-ap_r^2}{2\gamma m}\right] ,$$

(B1)

with $V(r)$ the potential derived from the radial force and $N_b$ the total number of electrons. This solution is dependent on finding a suitable temperature parameter $a$, such that the normalization of the distribution is preserved. For a potential which never exceeds that of a completely rarefied ion channel the parameter $a$ needs only to be increased from its nominal value, which simplifies the numerical approach.

We also make a provision for the radial tail of the beam to lie outside of the conducting wall radius, which was needed to solve the Maxwell equations. In this instance, we again call on the solenoid to help in stabilizing the computation, and assume that any beam particles outside of this radius are focused entirely by the solenoid. This approach is justified by the characteristically long tails of any Bennett-like radial profile.

[1] H. L. Buchanan, Phys. Fluids 30, 221 (1987).
[2] W. E. Martin, G. J. Caporaso, W. M. Fawley, D. Prosnitz, and A. G. Cole, Phys. Rev. Lett. 54, 685 (1985).
[3] K. Takayama and S. Hiramatsu, Phys. Rev. A 37, 173 (1988).
[4] J. Krall, K. Nguyen, and G. Joyce, Phys. Fluids B 1, 2099 (1989).
[5] E. P. Lee and R. K. Cooper, Part. Accel. 7, 83 (1976).
[6] D. A. Edwards and M. J. Syphers, in Physics of Particle Accelerators, edited by Melvin Month and Margaret Dienes, AIP Conf. Proc. No. 184 (AIP, New York, 1989), p. 2.
[7] H. Uhm and G. Joyce, Phys. Fluids B 3, 1587 (1991).
[8] J. J. Su, T. Katsouleas, J. M. Dawson, and R. Fedele, Phys. Rev. A 41, 3321 (1990).
[9] D. H. Whittum, Ph.D. thesis, University of California, Berkeley, 1990; and Lawrence Berkeley Laboratory Report No. 29720 (unpublished).
[10] J. B. Rosenzweig, T. Katsouleas, and J. J. Su, Phys. Rev. A 44, R6189 (1991).
[11] B. N. Breizman, T. Tajima, D. L. Fisher, and P. Z. Chebo-

taev (unpublished).
[12] J. B. Rosenzweig, P. Schoessow, C. Ho, W. Gai, R. Konecny, S. Mtingwa, J. Norem, M. Rosing, and J. Simpson, Phys. Fluids B 2, 1376 (1990).
[13] J. B. Rosenzweig et al., Phys. Rev. Lett. 61, 98 (1988); Phys. Rev. A 39, R1586 (1989).
[14] W. M. Sharp, M. Lampe, and H. S. Uhm, Phys. Fluids 257, 1456 (1982).
[15] E. P. Lee, Phys. Fluids 21, 1327 (1978).
[16] Handbook of Mathematical Functions, edited by M. Abramowitz and I. Stegun (Dover, New York, 1972), p. 721.
[17] P. Chen, K. Oide, A. M. Sessler, and S. S. Yu, Part. Accel. 31, 7 (1990).
[18] K. Oide, Phys. Rev. Lett. 61, 1713 (1988).
[19] R. Williams and T. Katsouleas, in Advanced Accelerator Concepts, edited by J. Wurtele, AIP Conf. Proc. No. 279 (AIP, New York, 1993).
[20] D. Whittum, W. Sharp, S. S. Yu, M. Lampe, and G. Joyce, Phys. Rev. Lett. 67, 991 (1991).